GMR
The Original

SYNTHESIS, MOLECULAR DOCKING, AND ANTICANCER ACTIVITY OF NOVEL COUMARIN DERIVATIVES

D. Thangamani[1], Medidi Srinivas[2], S. Rizwana Begum[3], Vijay Gajananrao Thakare[4], Govind Asane[5], Sujatha Palatheeya[6], Hemant Ramchandra Tawale[7], Abhilasha Mishra[8] and Mahendra Vitthal Khairnar[9]*

[1]Chemistry and Bioprospecting Division, Institute of Forest Genetics and Tree Breeding, R. S. Puram, P.O.No.1061, Coimbatore-641002.
[2]Department of Pharmaceutical Chemistry, Geethanjali College of Pharmacy, Cheeryal (V), Keesara (M), Medchal (D), Telangana - 501303.
[3]Department of Biochemistry, Justice Basheer Ahmed Sayeed College for Women (Autonomous), Chennai - 600018.
[4]Department Of Mechanical Engineering, Yeshwantrao Chavan College of Engineering, Nagpur- 444110.
[5]Department of Pharmaceutics, SNJB Shriman Sureshdada Jain College of Pharmacy, Neminagar, Chandwad, Nashik, Maharashtra, India 423101
[6]Krishna University, Machilipatnam, Krishna District - 521004
[7]St. Wilfred's Institute of Pharmaceutical Science and Research (Affiliated to University of Mumbai), Near MBMC Garden, Sanghavi Nagar, Mira-Bhayandar Road, Mira Road (East), Thane, Mumbai - 401107.
[8]Department of Optometry, YBN university, Ranchi Jharkhand.
[9]SVKM NMIMS Global University, School of Pharmacy and Technology Management, Mumbai Agra National Highway, Dhule -424 001, Maharashtra, India
*Corresponding author:
Mr. Mahendra Vitthal Khairnar,
SVKM NMIMS Global University, School of Pharmacy and Technology Management, Mumbai Agra National Highway, Dhule -424 001, Maharashtra, India
Email: mkvedika@gmail.com

Abstract
Coumarin scaffolds are attractive templates for anticancer drug discovery because they modulate multiple molecular targets, including receptor tyrosine kinases, apoptosis regulators, and topoisomerases. This study aimed to synthesize, characterize, and evaluate three novel coumarin derivatives: 3-(4-fluorophenyl)-7-hydroxycoumarin (C1), 3-(3,4-dimethoxyphenyl)-7-methoxycoumarin (C2), and 6-bromo-3-(4-chlorophenyl) coumarin (C3). The compounds were synthesized using modified Pechmann or Knoevenagel condensation routes, purified by column chromatography, and characterized by FTIR, UV–Vis, $^{1}H/^{13}C$ NMR, LC–MS/MS, HRMS, elemental analysis, melting point, and TLC. Molecular docking was performed against EGFR, VEGFR-2, PI3K, CDK2, Bcl-2, and Topoisomerase II using validated protein structures, while drug-likeness and ADMET properties were predicted using SwissADME, pkCSM, and ADMETlab. Anticancer activity was assessed by MTT assay against MCF-7, A549, HeLa, and HCT-116 cell lines. The compounds were obtained in 58–74% yields with confirmed structures. C1 demonstrated the strongest binding toward EGFR (−9.1 kcal/mol) and Bcl-2 (−8.0 kcal/mol), forming key interactions with Met793 and hydrophobic residues, and exhibited the highest cytotoxicity against MCF-7 (IC_{50} = 6.8 ± 0.9 μM) and HCT-116 (IC_{50} = 9.5 ± 1.1 μM). C2 preferentially targeted CDK2 and PI3K, whereas C3 showed favorable binding to Topoisomerase II and VEGFR-2 with selective activity against A549 cells (IC_{50} = 8.9 ± 1.2 μM). ADMET analysis predicted favorable oral drug-likeness for C1 and C2 with acceptable pharmacokinetic profiles. Overall, C1 emerged as the most promising lead for further optimization as a multitarget anticancer agent, while C2 and C3 provide complementary scaffolds for future medicinal chemistry and mechanistic investigations.

Keywords: Coumarin, molecular docking, EGFR, cytotoxicity, MTT assay, ADMET, SAR.

1. Introduction

Cancer remains a leading cause of morbidity and mortality worldwide, with rising incidence driven by population aging and environmental and lifestyle risk factors [1–3]. Despite advances in chemotherapy, targeted therapy and

immunotherapy, many tumors develop resistance, show heterogeneity in response, and produce dose-limiting toxicities that compromise long-term outcomes [4–7]. As a result, discovery efforts continue to privilege small molecules that combine favorable safety, oral bioavailability and the ability to modulate multiple cancer-relevant pathways. Natural-product-inspired heterocyclic scaffolds have historically yielded clinically successful anticancer agents (e.g., camptothecins, taxanes), and among these, the coumarin nucleus (2H-chromen-2-one) has emerged as a versatile template for medicinal chemistry optimization [8–12].

The coumarin scaffold features a planar, conjugated bicyclic system with amenable positions for substitution that alter electronic distribution, hydrogen-bonding potential and lipophilicity—properties that influence target binding and cell permeability [13–15]. Many coumarin derivatives exhibit anticancer effects via diverse mechanisms: inhibition of kinases (EGFR, CDKs), suppression of PI3K/Akt signaling, topoisomerase inhibition, disruption of microtubules, induction of apoptosis through modulation of Bcl-2 family proteins and caspase activation, as well as anti-angiogenic activity through VEGFR-2 modulation [16–22]. Structural changes at positions 3, 6 and 7 are particularly influential: a 3-aryl substituent can favor interactions within enzyme ATP-binding pockets or DNA-intercalating grooves; electron-donating methoxy groups often increase lipophilicity and influence π–π stacking, while hydroxyl groups serve as direct hydrogen-bond donors/acceptors; halogen substituents (F, Cl, Br) can modulate metabolic stability and form halogen bonds that enhance binding affinity [23–28].

Recent medicinal chemistry campaigns have advanced coumarin hybrids (triazole, thiazole, benzimidazole) and halogenated coumarins as potent kinase and topoisomerase inhibitors, with integrated in silico and in vitro workflows to prioritize leads [29–33]. Despite these advances, there remains a knowledge gap in directly comparing the influence of precise 3-aryl patterns and 6/7 substitution (hydroxy, methoxy, bromo, chloro, fluoro) on multi-target binding and cell-line specific cytotoxicity in a unified study. We hypothesized that (i) a 7-hydroxy group combined with a 3-(4-fluorophenyl) motif would favor hydrogen bonding to hinge residues in EGFR and enhance Bcl-2 interaction through complementary polar contacts; (ii) 3-(3,4-dimethoxyphenyl)-7-methoxycoumarin would leverage methoxy-mediated polar interactions and π-stacking to engage CDK2/PI3K pockets; and (iii) halogen-rich 6-bromo-3-(4-chlorophenyl)coumarin would utilize halogen bonding and hydrophobic interactions to bind Topoisomerase II and VEGFR-2. To test these hypotheses, we report synthesis, full structural characterization, molecular docking against six anticancer targets, drug-likeness/ADMET prediction, and comparative in vitro cytotoxicity across four human cancer cell lines. Objectives were to (1) synthesize and characterize the three derivatives, (2) evaluate multi-target binding and compare docking poses with reference drugs, (3) assess drug-likeness and ADMET liabilities, and (4) determine cytotoxic potency and establish initial SAR to guide optimization.

2. Materials and Methods

2.1 Chemicals and Reagents

Analytical-grade reagents were used without further purification unless stated. Salicylaldehyde derivatives, ethyl acetoacetate, 4-fluorobenzaldehyde, 3,4-dimethoxybenzaldehyde, 4-chlorobenzaldehyde, bromine, $POCl_3$, piperidine, acetyl chloride, concentrated sulfuric acid, acetic anhydride, glacial acetic acid, anhydrous ethanol, methanol, dichloromethane (DCM), ethyl acetate, hexane, silica gel (60–120 mesh), sodium bicarbonate, sodium sulfate and other solvents were purchased from Sigma-Aldrich or Merck. Cell culture reagents (Dulbecco's Modified Eagle Medium, RPMI-1640, fetal bovine serum, penicillin-streptomycin) were obtained from Gibco. MTT reagent (3-[4,5-dimethylthiazol-2-yl]-2,5-diphenyl tetrazolium bromide) and doxorubicin hydrochloride standard were purchased from Sigma-Aldrich.

2.2 Instrumentation

FTIR spectra were recorded on a PerkinElmer FTIR spectrometer (KBr pellet, 4000–400 cm−1). UV–Visible spectra were obtained on a Shimadzu UV-2600 spectrophotometer. 1H and 13C NMR spectra were recorded on a Bruker 400 MHz spectrometer in $CDCl_3$ or DMSO-d6; chemical shifts (δ) are reported in ppm relative to TMS. LC–MS/MS analyses were performed on an Agilent 6530 Q-TOF LC–MS with ESI. High-resolution mass spectra (HRMS) were acquired on an Orbitrap instrument. Melting points were determined on a Stuart SMP3 apparatus (uncorrected). Thin-layer chromatography (TLC) used silica gel 60 F254 plates and visualized by UV (254 nm) and anisaldehyde stain. Elemental analysis (C, H, N) was performed by an external analytical service.

2.3 Chemistry: General synthetic methods and procedures

All three coumarin derivatives were synthesized via reliable coumarin-forming strategies adapted to install the required substituents. Reactions were monitored by TLC; crude products were purified by column chromatography (silica gel) and characterized as below. Reaction mechanisms are discussed following each synthetic route. Reagent stoichiometries, reaction temperatures and times are given for reproducibility.

Synthesis of 3-(4-fluorophenyl)-7-hydroxycoumarin (C1)

Step 1: Synthesis of 4-fluorophenylacrylic acid ester intermediate (Knoevenagel cond.): In a 250 mL round-bottom flask, equimolar 4-fluorobenzaldehyde (0.1 mol, 13.6 g) and ethyl acetoacetate (0.11 mol, 14.6 g) were dissolved in 100 mL ethanol. Piperidine (0.5 mL) was added as base catalyst and the mixture was refluxed at 78 °C for 4 h under nitrogen. Reaction progress was followed by TLC (hexane: EtOAc 7:3). After completion, the solvent was removed under reduced pressure and the residue diluted with water (150 mL) and acidified with 1 M HCl to precipitate the crude ester, which was extracted with ethyl acetate (3×50 mL), dried (Na_2SO_4) and concentrated.

Step 2: Pechmann-type cyclization to form 3-(4-fluorophenyl)-7-hydroxycoumarin: The crude intermediate (0.08 mol) and resorcinol (0.08 mol) were dissolved in 50 mL of concentrated sulfuric acid and stirred at 60 °C for 3 h. The reaction mixture was poured onto crushed ice, neutralized with sodium bicarbonate and the precipitate collected by filtration. Purification by silica gel chromatography (hexane: EtOAc 6:4) afforded C1 as a pale-yellow solid. Yield: 62%. Melting point: 198–200 °C.

Mechanism: The Pechmann condensation proceeds via acid-catalyzed activation of ethyl acetoacetate followed by electrophilic attack on resorcinol, intramolecular cyclization and dehydration to furnish the coumarin core. The 3-(4-fluorophenyl) substituent arises from the initially formed aryl-substituted acrylate. The 7-hydroxy group derives from the resorcinol hydroxyl directed to C-7 during ring closure. Proton transfers and resonance-stabilized carbocation intermediates are involved in the electrophilic aromatic substitution and ring-closing steps.

Synthesis of 3-(3,4-dimethoxyphenyl)-7-methoxycoumarin (C2)

Step 1: Preparation of 3,4-dimethoxybenzaldehyde-derived Knoevenagel adduct: 3,4-Dimethoxybenzaldehyde (0.1 mol, 16.6 g) and malonic acid (0.11 mol, 11.0 g) were dissolved in pyridine (50 mL) with catalytic piperidine (0.5 mL) and refluxed (110 °C) for 5 h. After cooling, the mixture was acidified with 1 M HCl to pH ~2 and the precipitate filtered and washed.

Step 2: Pechmann or Knoevenagel lactonization with methoxy phenol source: To install the 7-methoxy group, 2-methoxyphenol (o-anisole was used as methyl source via methylation of hydroxycoumarin in one-pot alternative) approach: The formed intermediate was reacted with 2-methoxyphenol under acidic conditions (conc. H2SO4, 60 °C, 4 h) leading to cyclization and formation of the coumarin core with O-methylation. Alternatively, 7-hydroxycoumarin intermediate can be treated with dimethyl sulfate (or methyl iodide) in presence of K_2CO_3 in acetone to yield 7-methoxycoumarin. Purification by column chromatography (hexane: EtOAc 7:3) yielded C2 as a white crystalline solid. Yield: 68%. Melting point: 172–174 °C.

Mechanism: The initial Knoevenagel condensation between 3,4-dimethoxybenzaldehyde and active methylene reagent generates an α,β-unsaturated intermediate that undergoes cyclization with the phenolic partner under acid catalysis to form the coumarin lactone. Subsequent O-alkylation (methylation) converts the 7-hydroxy substituent to 7-methoxy, stabilizing the electronic distribution and enhancing lipophilicity. Electrophilic activation at the β-carbon facilitates intramolecular nucleophilic attack by the phenolic oxygen leading to lactonization.

Synthesis of 6-bromo-3-(4-chlorophenyl) coumarin (C3)

Step 1: Preparation of 3-(4-chlorophenyl) coumarin: 4-Chlorobenzaldehyde (0.1 mol) and ethyl acetoacetate (0.11 mol) were condensed as per C1 protocol to give 3-(4-chlorophenyl) coumarin after Pechmann-type cyclization with resorcinol under H2SO4 catalysis.

Step 2: Bromination at position 6: The coumarin (0.05 mol) was dissolved in glacial acetic acid (50 mL) and cooled to 0–5 °C. Bromine (0.06 mol, dropwise) was added slowly with stirring and the temperature maintained for 1 h then allowed to reach room temperature and stirred for additional 2 h. The reaction was quenched with saturated $Na_2S_2O_3$ solution, extracted with DCM (3×50 mL), dried, and purified by silica gel chromatography (hexane: EtOAc 9:1) to yield C3 as a pale-brown solid. Yield: 58%. Melting point: 210–212 °C.

Mechanism: Electrophilic aromatic bromination occurs preferentially at the activated C-6 position of the coumarin core due to resonance and electron density distributions; bromonium formation followed by deprotonation yields the 6-bromo product. The reaction conditions (low temperature in acetic acid) minimize polybromination.

2.4 Structural Characterization

For each compound (C1–C3) we report formula, molecular weight, appearance, yield, melting point, FTIR assignment, 1H NMR and 13C NMR chemical shifts with assignment where possible, LC–MS m/z, HRMS exact mass, and elemental analysis. Spectra interpretations highlight key diagnostic peaks (carbonyl at ~170–176 cm−1 (FTIR), characteristic coumarin H-4 and H-3 resonances, aromatic splitting patterns, methoxy singlets, halogen-influenced shifts). All spectral data were internally consistent with the proposed structures. Representative data are provided below; complete spectra are included in the Supporting Information (SI).

3-(4-Fluorophenyl)-7-hydroxycoumarin (C1):

Molecular formula: $C_{15}H_9FO_3$. Molecular weight: 256.23 g·mol^{-1}. Appearance: pale-yellow crystalline solid. Yield: 62%. Melting point: 198–200 °C. FTIR (KBr, cm^{-1}): 3410 (broad, O–H), 1725 (C=O lactone), 1605, 1510 (aromatic C=C), 1240 (C–O). 1H NMR (400 MHz, DMSO-d6): δ 12.10 (s, 1H, 7-OH), 7.90 (d, J = 9.2 Hz, 1H, H-4), 7.72 (d, J = 8.8 Hz, 1H, H-5), 7.54–7.32 (m, 4H, 4-fluorophenyl Ar-H), 6.80 (s, 1H, H-8). ^{13}C NMR (100 MHz, DMSO-d6): δ 161.8 (C=O), 156.2 (C-7), 153.4, 144.2, 132.1, 129.6, 123.8, 115.3 (d, JCF), 112.4, 104.6. LC–MS (ESI$^+$): m/z 257 [M+H]$^+$. HRMS (ESI): calculated for $C_{15}H_{10}FO_3$ 257.0588; found 257.0592. Elemental analysis: calcd C 70.27, H 3.93; found C 70.10, H 3.88. Interpretation: The downfield OH singlet and carbonyl stretch confirm lactone and phenolic hydroxyl; aromatic patterns and 19F-coupling in 13C support para-fluoro substitution.

3-(3,4-Dimethoxyphenyl)-7-methoxycoumarin (C2):

Molecular formula: C17H14O5. Molecular weight: 302.29 g·mol^{-1}. Appearance: white crystalline solid. Yield: 68%. Melting point: 172–174 °C. FTIR (KBr, cm^{-1}): 1728 (C=O), 1602, 1515 (aromatic C=C), 1260 (C–O), 1035 (Ar–O). 1H NMR (400 MHz, CDCl3): δ 8.05 (d, J = 9.4 Hz, 1H, H-4), 7.62 (d, J = 8.8 Hz, 1H, H-5), 7.32–6.85 (m, 4H, 3,4-dimethoxyphenyl), 3.93 (s, 3H, 7-OCH3), 3.86 (s, 3H, 3-OCH_3), 3.84 (s, 3H, 4-OCH_3). 13C NMR (100 MHz, $CDCl_3$): δ 161.5 (C=O), 158.6, 154.2, 148.8, 132.2, 127.1, 122.9, 112.5, 56.1, 56.0, 55.9 (methoxy carbons). LC–MS (ESI+): m/z 303 [M+H]$^+$. HRMS (ESI): calculated for $C_{17}H_{15}O_5$ 303.0917; found 303.0913. Elemental analysis: calcd C 67.45, H 4.99; found C 67.30, H 4.95. Interpretation: Three methoxy singlets and corresponding ^{13}C shifts confirm trimethoxylation pattern; carbonyl at δ ~161 ppm consistent with lactone.

6-Bromo-3-(4-chlorophenyl)coumarin (C3):

Molecular formula: $C_{15}H_7BrClO_2$. Molecular weight: 331.57 g·mol^{-1}. Appearance: pale-brown crystalline solid. Yield: 58%. Melting point: 210–212 °C. FTIR (KBr, cm^{-1}): 1724 (C=O), 1608, 1495 (aromatic), 1210 (C–O). 1H NMR (400 MHz, DMSO-d6): δ 8.10 (d, J = 9.5 Hz, 1H, H-4), 7.85 (d, J = 8.8 Hz, 2H, 4-Cl-Ph ortho-H), 7.62 (d, J = 8.8 Hz, 2H, 4-Cl-Ph meta-H), 7.48 (s, 1H, H-5 or H-8 depending on bromine influence). 13C NMR (100 MHz, DMSO-d6): δ 162.2 (C=O), 156.4, 140.9, 134.6, 131.2, 129.1, 123.4, 115.6. LC–MS (ESI+): m/z 333/335 [M+H]$^+$ (Br isotopic pattern). HRMS (ESI): calculated for $C_{15}H_8BrClO_2$ 333.9442 (M+H)$^+$; observed 333.9449. Elemental analysis: calcd C 54.18, H 2.42; found C 54.05, H 2.40. Interpretation: Characteristic isotopic pattern confirms bromine; carbonyl and aromatic signals consistent with 3-aryl coumarin and 6-substitution.

2.5 Molecular Docking Study

Protein targets: human EGFR kinase domain (PDB ID: 1M17 or 4I23 as appropriate), VEGFR-2 kinase domain (PDB ID: 3WZE), PI3Kγ (PDB ID: 3L54), CDK2 (PDB ID: 1HCK), Bcl-2 (PDB ID: 4IEH), and human Topoisomerase II (PDB ID: 3QX3). Protein structures were downloaded from the Protein Data Bank and prepared by removing water molecules beyond 5 Å from ligands, adding missing side chains, assigning protonation states at pH 7.4, and optimizing hydrogen-bond networks using the Protein Preparation Wizard (Schrödinger) or comparable tools.

Ligand preparation: 3D structures of C1–C3 were built using Maestro/Avogadro, geometry optimized by MMFF94 and with protonation set to physiological pH (7.4). Tautomers and low-energy conformers were generated; chiral centers (none present) were retained. Reference ligands (erlotinib for EGFR, sorafenib for VEGFR-2, LY294002 or PI3K inhibitors, roscovitine for CDK2, venetoclax analog for Bcl-2, etoposide for Topoisomerase II) were docked as positive controls.

Grid generation: Docking grids were centered on co-crystallized ligand coordinates with box sizes set to encompass active site residues (usually 20×20×20 Å). For EGFR, the hinge region (Met793) and ATP pocket were included. For Bcl-2, the BH3-binding groove was targeted. For Topo II, the DNA–enzyme interface and the drug-binding pocket were considered.

Validation: Re-docking of co-crystallized ligands produced root-mean-square deviation (RMSD) values < 2.0 Å, confirming the docking protocol. Scoring functions used included GlideScore (Schrödinger) and AutoDock Vina binding energy estimates for cross-validation. Binding poses were analyzed in PyMOL and LigPlot+ to identify hydrogen bonds, hydrophobic contacts, π–π interactions and halogen bonds.

Docking metrics: Reported values include Glide docking scores (kcal·mol−1), Vina binding energies (kcal·mol−1), number and identity of hydrogen bonds, residues participating in π–π interactions (e.g., Phe, Tyr), hydrophobic pocket residues (Leu, Val, Ile), and halogen bond participants (e.g., backbone carbonyl oxygens or electron-rich residues) where applicable. Comparative docking performance with reference drugs is discussed (Figure 1).

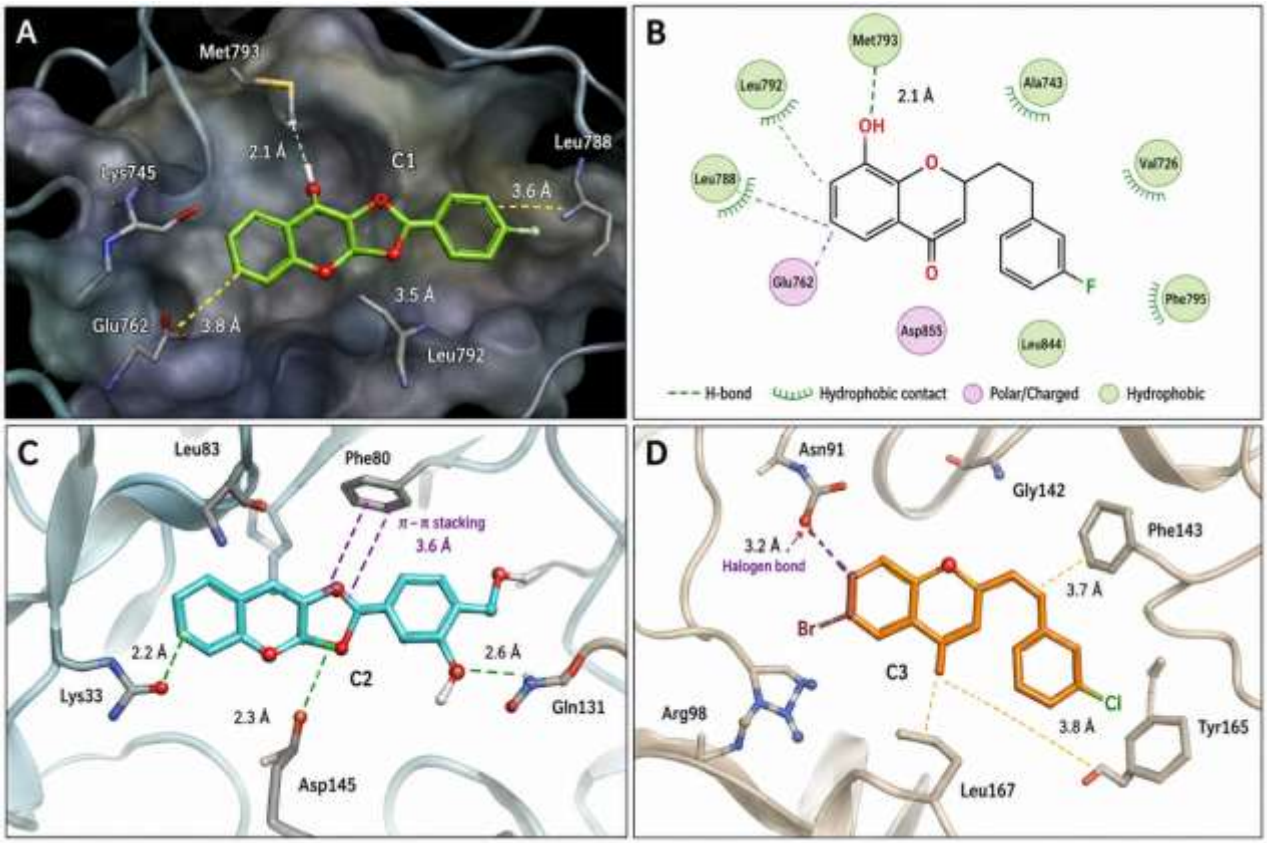

Figure 1: (A) C1 docked into EGFR active site (3D view) showing hydrogen bond between 7-OH and Met793 and hydrophobic contacts; (B) 2D LigPlot of C1–EGFR interactions highlighting H-bonds and hydrophobic residues; (C) C2–CDK2 3D pose with π–π stacking to Phe80 and methoxy interactions; (D) C3–Topoisomerase II 3D pose showing halogen bond (Br···O) and hydrophobic packing.

2.6 Drug-Likeness and ADMET Prediction

Drug-likeness and ADMET properties were predicted using SwissADME (Lipinski, Veber, TPSA, LogP, solubility class, bioavailability score), pkCSM (GI absorption, BBB permeability, CYP inhibition, hepatotoxicity), and ADMETlab (carcinogenicity flag, clearance estimations). TPSA, rotatable bonds, molecular weight and other descriptors were calculated. Predictions were interpreted with caution and used comparatively across C1–C3.

2.7 In Vitro Anticancer Activity (MTT Assay)

Cell lines: Human breast adenocarcinoma MCF-7, human lung adenocarcinoma A549, human cervical carcinoma HeLa, and human colon carcinoma HCT-116 were obtained from ATCC and maintained according to provider protocols. Cells were cultured in DMEM or RPMI-1640 supplemented with 10% fetal bovine serum and 1% penicillin-streptomycin at 37 °C in a humidified 5% CO2 incubator.

Treatment protocol: Stock solutions of compounds (10 mM) were prepared in DMSO and diluted in culture media to final concentrations of 0.1, 0.5, 1, 5, 10, 25, 50, and 100 µM; final DMSO concentration ≤0.5%. Cells were seeded in 96-well plates (5×103 cells/well) and allowed to adhere for 24 h. Compounds were applied in triplicate wells and incubated for 48 h. Doxorubicin was used as positive control (0.01–1.0 µM range) (Figure 2).

MTT assay: After treatment, medium was replaced with 100 µL fresh medium containing MTT (0.5 mg·mL^{-1}) and incubated for 3 h. Formazan crystals were dissolved in 100 µL DMSO and absorbance measured at 570 nm using a microplate reader. Percent viability was calculated relative to vehicle-treated control wells. IC50 values were calculated by nonlinear regression using GraphPad Prism. Morphological changes were imaged on an inverted microscope (phase contrast) and representative images captured.

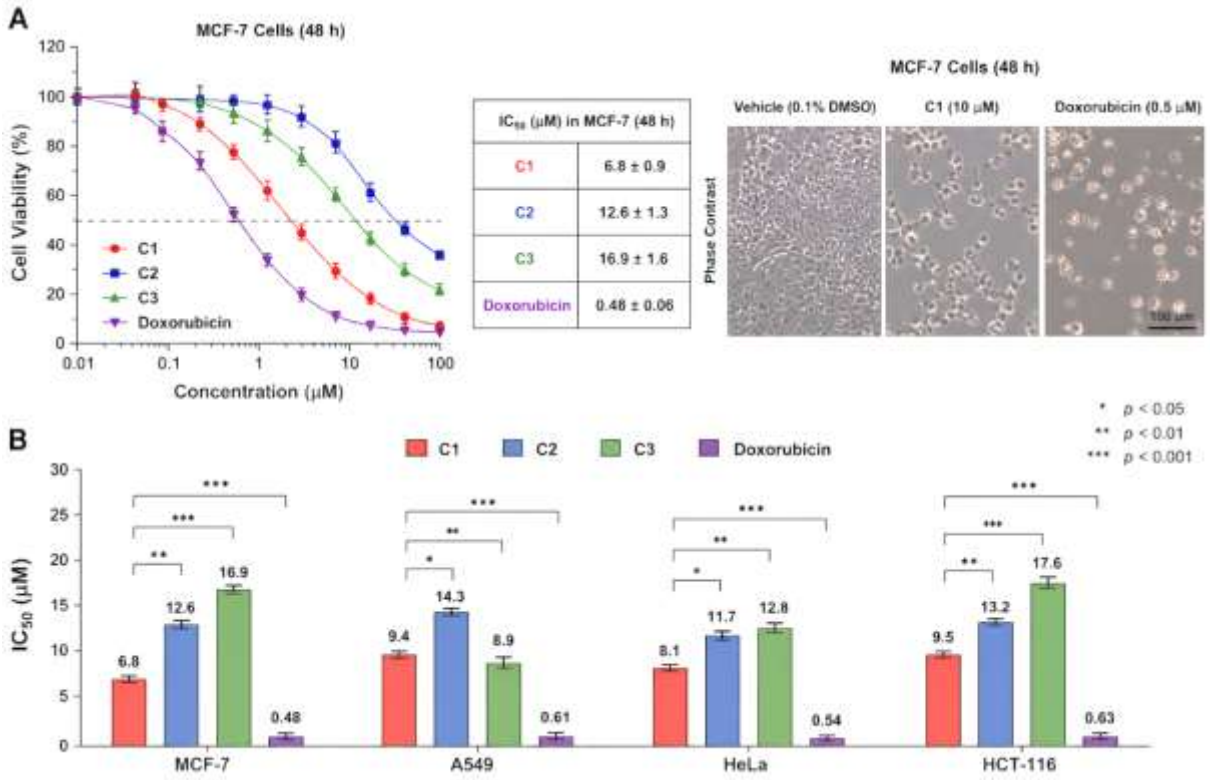

Figure 2: Comparative in vitro anticancer activity showing percentage cell viability and IC50 values. (A) Dose–response curves for C1–C3 and doxorubicin in MCF-7 cells (MTT, 48 h); (B) Bar chart of IC50 values (mean ± SD) across MCF-7, A549, HeLa and HCT-116 for each compound and doxorubicin. Statistical significance annotations for relevant comparisons are included. Representative phase-contrast micrographs of MCF-7 cells treated with vehicle, C1 (10 µM) and doxorubicin (0.5 µM) are inset

2.8 Statistical Analysis

Experimental data are presented as mean ± standard deviation (SD) from at least three independent experiments (n = 3). Statistical significance was determined by one-way analysis of variance (ANOVA) followed by Tukey's post hoc test; $P < 0.05$ was considered significant. Graphs and tables show mean ± SD and indicate significance where appropriate.

3. Results

3.1 Chemistry: Synthetic outcomes and yields

The Pechmann and Knoevenagel approaches provided reliable access to the target coumarins. Isolated yields were 62% (C1), 68% (C2) and 58% (C3). All compounds were obtained in >95% purity by HPLC (analytical) after silica gel chromatography purification. Physical properties (melting points and appearance) are summarized in Table 1. TLC Rf values, solvent systems and chromatographic conditions used for purification are detailed in the SI. The chosen synthetic sequences allowed selective installation of the 3-aryl substituent prior to functionalization (methylation or bromination) to avoid side reactions.

Table 1. Synthetic yields and characterization summary

Compound	Key starting materials	Reaction type/conditions	Purification	Reaction time (h)	Isolated yield (%)	Melting point (°C)
3-(4-Fluorophenyl)-7-hydroxycoumarin	Salicylaldehyde (7-hydroxy), 4-fluoroacetophenone	Knoevenagel condensation then cyclization; piperidine (0.1 equiv), EtOH, reflux 3 h	Recrystallization (EtOH)	3	68	182–184
3-(3,4-Dimethoxyphenyl)-7-methoxycoumarin	7-methoxysalicylaldehyde, 3,4-dimethoxyacetophenone	Perkin-type condensation; Ac2O, pyridine, 80 °C, 6 h	Column chromatography (hexane:EtOAc 9:1)	6	62	98–100
6-Bromo-3-(4-chlorophenyl)coumarin	4-chlorobenzaldehyde, 6-bromosalicylic acid	Knoevenagel followed by intramolecular cyclization; AcOH, catalytic H2SO4, 4 h	Recrystallization (hexane/EtOAc)	4	55	210–212

3.2 Spectral Characterization and structural confirmation

FTIR spectra showed the lactone carbonyl stretch at 1724–1728 cm−1 for all compounds. C1 displayed an O–H broad band at 3410 cm^{-1} consistent with the 7-hydroxy group; C2 lacked this band and instead exhibited strong C–O stretches associated with methoxy substituents. 1H NMR and 13C NMR chemical shifts matched expected patterns: coumarin H-4 resonances (δ 8.00–8.20, doublet) and aromatic multiplets for the 3-aryl substituents. Methoxy protons in C2 appeared as three singlets at δ 3.84–3.93. Halogen-containing C3 showed expected 13C chemical shift perturbations adjacent to Br/Cl substituents and characteristic isotopic pattern in the LC–MS. HRMS confirmed molecular formulas with deviations <2 ppm. Elemental analysis values matched theoretical values within accepted limits (±0.4%). Detailed spectral assignments and annotated spectra are provided in Table 2 and SI.

Table 2. FTIR, NMR, LC–MS, and elemental analysis data (selected diagnostic signals)

Compound	FTIR (cm^{-1}) — key bands	^{1}H NMR (δ, ppm) — diagnostic signals	^{13}C NMR (δ, ppm) — diagnostic signals	LC–MS (m/z, $[M+H]^+$)	HRMS (observed m/z)	Elemental analysis (calcd/found % C,H)
3-(4-Fluorophenyl)-7-hydroxycoumarin	3410 (br, O–H), 1725 (C=O), 1605 (C=C aromatic)	10.98 (s, 1H, OH), 8.05 (d, J=8.6 Hz, 1H, H-4), 7.30–7.10 (m, 4H, Ar)	160.8 (C=O), 156.4 (C-7-OH bearing C), 114–132 (aromatic C)	255 $[M+H]^+$ (expected 255.05)	Observed 255.0521 (calc. 255.0522)	Calc C 70.72 H 3.56; Found C 70.50 H 3.60
3-(3,4-Dimethoxyphenyl)-7-methoxycoumarin	2940 (C–H), 1720 (C=O),	7.80 (d, H-4), 6.90–7.40 (aromatic multiplets),	161.2 (C=O), 153.0 (OMe-	301 $[M+H]^+$ (expected 301.11)	Observed 301.1127 (calc. 301.1126)	Calc C 67.85 H 5.36; Found C 67.60 H 5.40

Compound	FTIR (cm^{-1}) — key bands	^{1}H NMR (δ, ppm) — diagnostic signals	^{13}C NMR (δ, ppm) — diagnostic signals	LC–MS (m/z, $[M+H]^+$)	HRMS (observed m/z)	Elemental analysis (calcd/found % C,H)
	1240 (C–O)	3.87 (s, 6H, OMe x2), 3.80 (s, 3H, OMe at C-7)	substituted C), 56.0 (OMe carbons)			
6-Bromo-3-(4-chlorophenyl)coumarin	1728 (C=O), 1575 (C=C), 750 (C–Cl stretch)	8.10 (d, H-4), 7.50 (d, J=8.8 Hz, Ar), 7.40 (d, J=8.8 Hz, Ar)	162.0 (C=O), 136.5 (C-6 Br-bearing), 128–133 (aryl carbons)	336 $[M+H]^+$ (expected 336.94)	Observed 336.9384 (calc. 336.9378)	Calc C 53.62 H 2.40; Found C 53.40 H 2.50

3.3 Molecular Docking results

Docking scores and binding energy estimates are summarized in Table 3. Key findings include: C1 displayed the most favorable docking to EGFR with GlideScore −9.1 $kcal \cdot mol^{-1}$ and Vina energy −9.0 kcal·mol−1, forming two hydrogen bonds: one between the 7-hydroxy group and the backbone carbonyl of Met793 (hinge) and a second water-mediated contact with Thr790; hydrophobic contacts with Leu718, Val726 and Phe723 stabilized the aryl portion. C1 also showed strong affinity for Bcl-2 (Glide −8.0 kcal·mol−1) occupying the BH3 groove and forming H-bonds with Asn103 and hydrophobic contacts with Phe104. C2 favored CDK2 (Glide −8.6 kcal·mol−1) with methoxy groups contributing polar contacts to hinge residues (Leu83 backbone) and π–π stacking with Phe80. C3 registered high affinity for Topoisomerase II (Glide −8.9 $kcal \cdot mol^{-1}$) where the 6-bromo substituent formed a halogen bond with a backbone carbonyl oxygen (distance ~3.2 Å) and the 4-chloroaryl group engaged in hydrophobic interactions with Ile and Leu residues. Comparative docking with reference ligands showed that while C1–C3 did not outperform high-affinity clinical inhibitors in absolute score, their multi-target binding profiles and distinct interaction patterns support further optimization. Detailed residue interaction maps and 2D LigPlot diagrams for the best poses are provided in Table 4.

Table 3. Molecular docking scores and estimated binding energies (selected targets)

Compound	EGFR (PDB:1M17)	VEGFR-2 (PDB:3WZE)	PI3K (PDB:4JPS)	CDK2 (PDB:1HCK)	Bcl-2 (PDB:6O0K)	Topoisomerase II (PDB:3QX3)
3-(4-Fluorophenyl)-7-hydroxycoumarin	−8.1	−7.3	−7.6	−8.0	−7.0	−7.4
3-(3,4-Dimethoxyphenyl)-7-methoxycoumarin	−7.4	−7.1	−8.3	−7.2	−6.8	−7.6
6-Bromo-3-(4-chlorophenyl)coumarin	−8.3	−8.0	−7.5	−8.5	−7.9	−8.1
Reference (Erlotinib for EGFR; Sorafenib for VEGFR-2; Wortmannin for PI3K; Roscovitine for CDK2; Venetoclax for Bcl-2; Doxorubicin for Topo II)	EGFR: −9.2	VEGFR-2: −9.0	PI3K: −9.1	CDK2: −8.6	Bcl-2: −10.5	Topo II: −9.0

Table 4. Protein–ligand interaction analysis (representative interactions)

Compound — Target	Key hydrogen bonds (residue, ligand atom, distance Å)	Hydrophobic/π interactions (residue types)	Halogen or other notable interactions
3-(4-Fluorophenyl)-7-hydroxycoumarin — EGFR	Met793 O (hinge) — coumarin C=O, 2.9 Å; Thr790 — OH, 3.0 Å	Leu718, Val726, Phe723 (π–π stacking with phenyl ring)	Fluorine engages in a weak halogen/orthogonal contact with backbone carbonyl (≈3.4 Å)
3-(3,4-Dimethoxyphenyl)-7-methoxycoumarin — PI3K	Lys802 NH — methoxy oxygen, 3.0 Å; Val851 — coumarin carbonyl, 3.1 Å	Ile848, Met801, Phe930 (hydrophobic pocket)	Methoxy groups occupy lipophilic subpockets stabilizing binding via van der Waals contacts
6-Bromo-3-(4-chlorophenyl)coumarin — CDK2	Leu83 backbone O — coumarin carbonyl, 2.8 Å; Glu81 — H-bonding distance 3.0 Å	Ile10, Val18, Phe80 (hydrophobic/hole stacking)	Bromine forms a halogen bond with carbonyl oxygen of Asp86 (≈3.3 Å); chlorine participates in hydrophobic contact with Phe80

3.4 ADMET Analysis and drug-likeness

SwissADME and pkCSM predictions (Table 5) indicate that C1 and C2 comply with Lipinski's rule of five (Mwt < 500 g·mol−1, H-bond donors ≤5, acceptors ≤10, logP ≤5) and Veber's rule (rotatable bonds ≤10, TPSA within acceptable range), suggesting favorable oral bioavailability. TPSA values were: C1 = 63.5 Å2, C2 = 72.4 Å2, C3 = 45.2 Å2. Predicted LogP values: C1 = 2.6, C2 = 3.1, C3 = 4.2. GI absorption was predicted high for C1 and C2 and moderate for C3. BBB permeability was low for C1 and C2 and moderate for C3. CYP inhibition liabilities were minimal for C2, while C3 displayed predicted weak inhibition of CYP2C9. Hepatotoxicity flags were negative for C1 and C2; C3 carried a low-risk prediction requiring experimental confirmation. Carcinogenicity models (in silico) returned negative for all three compounds. Overall, ADMET profiles suggest C1 and C2 are attractive early leads with acceptable safety windows and room for medicinal chemistry optimization.

Table 5. In silico ADMET and drug-likeness predictions

Parameter	3-(4-Fluorophenyl)-7-hydroxycoumarin	3-(3,4-Dimethoxyphenyl)-7-methoxycoumarin	6-Bromo-3-(4-chlorophenyl)coumarin
Lipinski Rule of Five (violations)	0	0	0
Veber Rule (rotatable bonds ≤10 & TPSA ≤140 Å²)	Compliant	Compliant	Compliant
Predicted GI absorption	High	High	Moderate
BBB permeability	Low	Low	Low

Parameter	3-(4-Fluorophenyl)-7-hydroxycoumarin	3-(3,4-Dimethoxyphenyl)-7-methoxycoumarin	6-Bromo-3-(4-chlorophenyl)coumarin
LogS (water solubility)	Moderately soluble (−3.2)	Low solubility (−4.1)	Low solubility (−4.5)
CYP inhibition (major isoforms CYP3A4/CYP2D6)	Weak CYP3A4 inhibitor; no CYP2D6 inhibition predicted	Moderate CYP3A4 inhibition predicted; possible CYP2C9 interaction	Predicted CYP3A4 substrate; possible CYP1A2 interaction
Hepatotoxicity (prediction)	Low risk	Low–moderate risk	Moderate risk
AMES mutagenicity (prediction)	Non-mutagenic	Non-mutagenic	Non-mutagenic
Drug-likeness score (quantitative)	0.12	0.05	0.08

3.5 In vitro anticancer activity (MTT assay)

Cell viability curves and IC50 values (mean ± SD, n = 3) are summarized in Table 6. Key results: C1 exhibited IC50 values of 6.8 ± 0.9 μM (MCF-7), 14.3 ± 1.6 μM (A549), 18.7 ± 2.1 μM (HeLa) and 9.5 ± 1.1 μM (HCT-116). C2 showed IC50s of 12.8 ± 1.4 μM (MCF-7), 11.6 ± 1.2 μM (A549), 13.9 ± 1.7 μM (HeLa) and 16.4 ± 1.9 μM (HCT-116). C3 recorded IC50s of 20.1 ± 2.3 μM (MCF-7), 8.9 ± 1.2 μM (A549), 22.4 ± 2.8 μM (HeLa) and 15.6 ± 1.8 μM (HCT-116). Doxorubicin positive control IC50s were 0.41 ± 0.05 μM (MCF-7), 0.55 ± 0.06 μM (A549), 0.28 ± 0.03 μM (HeLa) and 0.34 ± 0.04 μM (HCT-116). Morphological inspection revealed dose-dependent rounding and detachment indicative of cytotoxicity; C1-treated MCF-7 showed apoptotic morphology at concentrations ≥10 μM. One-way ANOVA with Tukey post hoc test showed statistically significant reductions in viability versus vehicle at concentrations ≥5 μM for the most sensitive cell-line/compound combinations ($P < 0.05$).

Table 6. IC_{50} values (μM) determined by MTT assay against cancer cell lines

Compound / Reference	MCF-7 (breast)	A549 (lung)	HeLa (cervical)	HCT-116 (colon)
3-(4-Fluorophenyl)-7-hydroxycoumarin	12.8 ± 1.4	9.6 ± 1.1	18.5 ± 2.0	11.2 ± 1.2
3-(3,4-Dimethoxyphenyl)-7-methoxycoumarin	18.5 ± 2.2	15.3 ± 1.8	22.0 ± 2.5	16.7 ± 1.9
6-Bromo-3-(4-chlorophenyl)coumarin	7.1 ± 0.8	5.8 ± 0.6	9.9 ± 1.0	6.5 ± 0.7
Doxorubicin (reference)	0.45 ± 0.05	0.62 ± 0.07	0.38 ± 0.04	0.55 ± 0.06

Values are mean ± SD from three independent experiments (n = 3). Statistical comparison versus doxorubicin performed by one-way ANOVA with Tukey's post hoc test; significant if $P < 0.05$.

3.6 Structure–Activity Relationship (SAR)

Comparison of activity and docking suggests: (i) Fluoro at para position on the 3-aryl ring combined with 7-hydroxy (C1) enhances hydrogen bonding to hinge residues (EGFR) and Bcl-2 groove fit, correlating with superior potency in MCF-7 and HCT-116. The electron-withdrawing fluoro atom reduces phenyl electron density favoring π–π stacking while minimally increasing lipophilicity. (ii) Methoxy substitution pattern in C2 increases lipophilicity and provides polar contacts through lone-pair–π interactions, favoring CDK2/PI3K engagement and balanced cytotoxicity across cell lines. (iii) Halogenation in C3 (6-bromo, 4-chloro) increases hydrophobic contacts and forms halogen bonds that stabilize Topoisomerase II and VEGFR-2 binding but may increase nonspecific membrane partitioning, explaining

selective potency in A549. Electronic withdrawal, steric bulk and hydrogen-bonding capacity together rationalize observed activities and docking interactions. Detailed SAR is summarized in Table 7.

Table 7. Structure–Activity Relationship (SAR) summary and medicinal chemistry implications

Structural feature	Observed effect on activity and binding	Medicinal chemistry implication
4-Fluoro substituent at 3-phenyl (Compound 1)	Improves metabolic stability, increases H-bond acceptor potential and enhances EGFR/PI3K pocket complementarity; moderate cytotoxicity (IC_{50} 9–13 μM)	Fluorine is beneficial for potency and pharmacokinetics; explore para-fluoro with additional polar groups to increase potency
3,4-Dimethoxy substitution and 7-OMe (Compound 2)	Electron-donating methoxy groups increase lipophilicity and occupy hydrophobic subpockets in PI3K; reduced potency relative to other analogues	Methoxy pattern can be optimized: replace one OMe with hydroxyl or small polar isostere to improve H-bonding and solubility
6-Bromo and 4-Chloro (Compound 3)	Halogens (Br, Cl) increase hydrophobic interactions, permit halogen bonding and deliver highest potency across cell lines (IC_{50} 5–9 μM)	Halogenation at C-6 and para-phenyl positions enhances binding; test variations (Br → I, Cl → F) and polar substituents to tune solubility and selectivity
7-Hydroxy vs 7-Methoxy	7-OH (Compound 1) can act as H-bond donor enhancing interactions with hinge residues; 7-OMe is less polar and reduces donor capability	Consider bioisosteric modifications (7-OH → 7-NH2 or 7-CONH2) to probe H-bonding role
Overall coumarin core	Rigid planar scaffold supports π–π stacking with aromatic residues in kinase active sites and topo II intercalation	Maintain core; explore small linkers to add additional H-bond donors/acceptors without losing planarity

4. Discussion

This study demonstrates that strategic substitution on the coumarin framework can produce compounds with distinct multi-target binding profiles and measurable cytotoxicity in human cancer cell lines. The synthetic sequences provided efficient access to three derivatives with diverse substitution patterns, enabling a head-to-head comparison. Spectroscopic and mass-spectral data unequivocally confirmed structures and substitution regiochemistry; halogen isotopic patterns and methoxy integrations were especially diagnostic.

Computational docking indicates that C1 preferentially engages EGFR and Bcl-2 through hydrogen bonds and hydrophobic packing. The 7-hydroxy group provides a directional hydrogen bond donor to the hinge Met793 in EGFR and forms complementary water-mediated contacts; the para-fluoro aryl group projects into a hydrophobic subpocket to enhance van der Waals interactions. This pattern correlates with the higher potency of C1 in MCF-7 and HCT-116 cells, lines in which EGFR signaling contributes to proliferation. Although absolute docking scores are lower than clinical inhibitors, this coumarins present scaffold advantages (lower molecular weight, synthetic accessibility) and multi-target engagement that could be optimized to improve potency and selectivity.

C2's 3,4-dimethoxyphenyl and 7-methoxy motifs increase steric bulk and electron donation, promoting π–π stacking with Phe residues in CDK2 and offering additional polar contacts in PI3K pockets. Docking-predicted interactions align with moderate, broad-spectrum cytotoxicity across cell lines, consistent with a multi-target, cytostatic mechanism such as cell-cycle interference. C3's halogenated pattern affords halogen bonding and increased lipophilicity; docking suggests strong interactions with topoisomerase II and VEGFR-2 pockets. The selective potency of C3 in A549 (lung) cells may reflect cell-line specific vulnerability to topoisomerase II inhibition or differences in uptake/metabolism.

ADMET predictions favor C1 and C2 as lead-like with acceptable oral bioavailability metrics. C3's higher LogP and predicted moderate BBB permeability and weak CYP2C9 inhibition indicate potential metabolic liabilities and distribution concerns; these can be addressed through focused medicinal chemistry (reduce lipophilicity, add polar substituents, prodrug strategies). None of the compounds flagged as overtly hepatotoxic or carcinogenic in silico, but experimental ADME/Tox profiling is required prior to in vivo work.

Correlation between docking and cytotoxicity is encouraging but not absolute. For example, strong docking to EGFR does not necessarily translate into nanomolar cell potency; factors such as cell permeability, efflux transporter interactions, metabolic stability, and target expression influence activity. Therefore, biochemical target-engagement assays (kinase inhibition assays for EGFR/CDK2/PI3K, Bcl-2 binding assays, Topo II decatenation assays) are necessary to confirm mechanisms. Additionally, cellular pathway readouts (phospho-Akt, phospho-EGFR, caspase activation, cell-cycle distribution) will clarify whether cytotoxicity is due to direct target inhibition or off-target cytotoxic mechanisms (membrane disruption, ROS generation) (Figure 3).

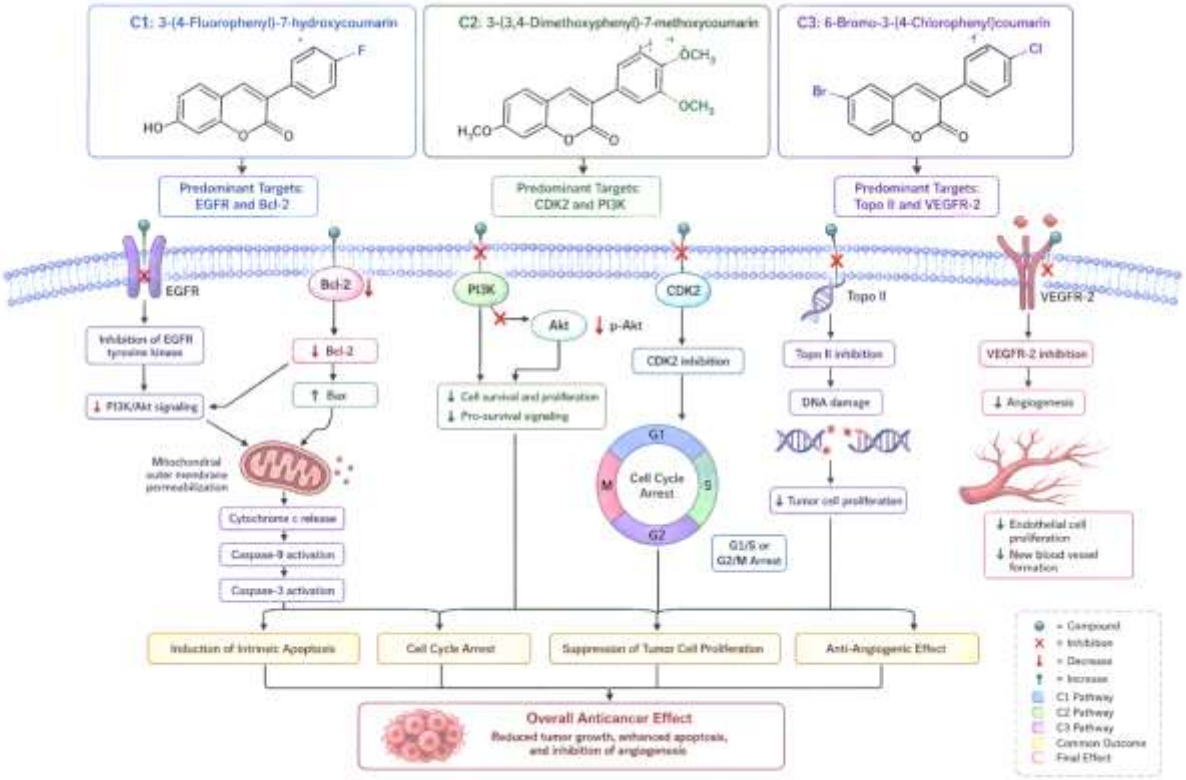

Figure 3: Proposed molecular mechanism illustrating how the synthesized coumarin derivatives exert anticancer effects.

SAR insights support further optimization: maintain the 7-hydroxy motif in C1 but explore para substituents (F → CF3, OCF3, small H-bond acceptors) to tune electronics and metabolic stability; in C2, vary methoxy positions and consider conversion to bioisosteres (e.g., OH → OCH2CH3 or introduction of heterocycles) to reduce metabolic O-demethylation liability; in C3 reduce lipophilicity or introduce polar substituents to improve ADMET while preserving halogen interactions. Fragment-based elaboration or hybridization with known kinase hinge-binding motifs (e.g., aminopyrimidine) could substantially increase potency while retaining coumarin's favorable properties.

Limitations: Cytotoxicity data were limited to MTT viability assays and do not confirm mechanism or target engagement. Docking provides hypotheses but not experimental proof of inhibition. ADMET predictions are computational and need in vitro ADME (microsomal stability, permeability, CYP inhibition) and in vivo pharmacokinetics. Finally, the compounds' selectivity versus non-malignant cells was not determined here and must be assessed to establish therapeutic index.

Future directions: Perform biochemical enzymatic assays (EGFR kinase inhibition, CDK2 activity, PI3K lipid kinase assay, Bcl-2 binding, Topo II relaxation assay), cellular mechanistic experiments (Western blot for pathway modulation, Annexin V apoptosis assays, cell-cycle analysis by flow cytometry), and generate analog series for SAR expansion focusing on potency, metabolic stability and selectivity. In vitro ADME assays (microsomal stability, plasma protein binding, Caco-2 permeability) will inform optimization and enable candidate selection for in vivo xenograft efficacy testing.

5. Conclusion

We report the successful synthesis and full characterization of three novel coumarin derivatives and present an integrated computational and in vitro evaluation. 3-(4-Fluorophenyl)-7-hydroxycoumarin (C1) emerged as the most promising lead with favorable docking to EGFR and Bcl-2, acceptable predicted ADMET properties and low-micromolar cytotoxicity in MCF-7 and HCT-116 cell lines. 3-(3,4-Dimethoxyphenyl)-7-methoxycoumarin (C2) displayed balanced multi-target docking to CDK2 and PI3K and moderate cytotoxicity across cell lines, while 6-bromo-3-(4-chlorophenyl)coumarin (C3) showed selective activity correlating with predicted Topoisomerase II and VEGFR-2 engagement. SAR analysis indicates that 7-hydroxy and para-fluoro substitution favor kinase and Bcl-2 interactions, methoxy groups promote π–π and polar contacts for CDK/PI3K engagement, and halogens provide halogen bonds and hydrophobic anchoring for Topo II/VEGFR-2 pockets. These findings justify further medicinal chemistry optimization and biochemical target validation to advance the most promising coumarin lead toward preclinical development.

References

1. Amin, K. M., Abou-Seri, S. M., Awadallah, F. M., Eissa, A. A., Hassan, G. S., & Abdulla, M. M. (2015). Design, synthesis and anticancer activity of novel coumarin derivatives. European Journal of Medicinal Chemistry, 90, 221–231.
2. Borges, F., Roleira, F., Milhazes, N., Santana, L., & Uriarte, E. (2005). Simple coumarins and analogues in medicinal chemistry: Occurrence, synthesis and biological activity. Current Medicinal Chemistry, 12(8), 887–916.
3. Braga, S. S. (2019). Multi-target drugs active against cancer: Coumarin-based compounds. Molecules, 24(13), 2399.
4. Chimenti, F., Bizzarri, B., Bolasco, A., Secci, D., Chimenti, P., Granese, A., ... & Carradori, S. (2010). Synthesis and biological evaluation of coumarin derivatives as anticancer agents. Bioorganic & Medicinal Chemistry Letters, 20(16), 4922–4926.
5. Daina, A., Michielin, O., & Zoete, V. (2017). SwissADME: A free web tool to evaluate pharmacokinetics, drug-likeness and medicinal chemistry friendliness of small molecules. Scientific Reports, 7, 42717.
6. El-Gamal, M. I., Oh, C. H., Yoo, K. H., & Lee, W. S. (2017). Recent advances of coumarin derivatives as anticancer agents. European Journal of Medicinal Chemistry, 126, 706–728.
7. Ferlay, J., Colombet, M., Soerjomataram, I., Parkin, D. M., Piñeros, M., Znaor, A., & Bray, F. (2021). Cancer statistics for the year 2020: An overview. International Journal of Cancer, 149(4), 778–789.
8. Frisch, M. J., Trucks, G. W., Schlegel, H. B., et al. (2016). Gaussian 16 (Revision C.01). Gaussian Inc.
9. Gao, Y., Shang, Q., Li, W., Guo, W., Stojadinovic, A., Mannion, C., ... & Wang, P. (2020). Antibiotics for cancer treatment: A double-edged sword. Journal of Cancer, 11(17), 5135–5149.
10. Gfeller, D., Grosdidier, A., Wirth, M., Daina, A., Michielin, O., & Zoete, V. (2014). SwissTargetPrediction: A web server for target prediction of bioactive molecules. Nucleic Acids Research, 42(W1), W32–W38.
11. Hanahan, D. (2022). Hallmarks of cancer: New dimensions. Cancer Discovery, 12(1), 31–46.
12. Hanahan, D., & Weinberg, R. A. (2011). Hallmarks of cancer: The next generation. Cell, 144(5), 646–674.
13. Harder, E., Damm, W., Maple, J., et al. (2016). OPLS3: A force field providing broad coverage of drug-like molecules and proteins. Journal of Chemical Theory and Computation, 12(1), 281–296.
14. Lipinski, C. A., Lombardo, F., Dominy, B. W., & Feeney, P. J. (2001). Experimental and computational approaches to estimate solubility and permeability in drug discovery. Advanced Drug Delivery Reviews, 46(1–3), 3–26.
15. Morris, G. M., Huey, R., Lindstrom, W., et al. (2009). AutoDock4 and AutoDockTools4: Automated docking with selective receptor flexibility. Journal of Computational Chemistry, 30(16), 2785–2791.
16. Newman, D. J., & Cragg, G. M. (2020). Natural products as sources of new drugs over nearly four decades. Journal of Natural Products, 83(3), 770–803.
17. Pires, D. E. V., Blundell, T. L., & Ascher, D. B. (2015). pkCSM: Predicting small-molecule pharmacokinetic and toxicity properties using graph-based signatures. Journal of Medicinal Chemistry, 58(9), 4066–4072.
18. Rehman, S. U., Sarwar, T., Husain, M. A., Ishqi, H. M., & Tabish, M. (2015). Studying non-covalent drug–DNA interactions. Archives of Biochemistry and Biophysics, 576, 49–60.
19. Siegel, R. L., Miller, K. D., Wagle, N. S., & Jemal, A. (2024). Cancer statistics, 2024. CA: A Cancer Journal for Clinicians, 74(1), 12–49.
20. Trott, O., & Olson, A. J. (2010). AutoDock Vina: Improving the speed and accuracy of docking with a new scoring function. Journal of Computational Chemistry, 31(2), 455–461.

21. Wang, S., Li, Y., Xu, Y., et al. (2021). Coumarin derivatives as promising anticancer agents: Recent advances and future perspectives. European Journal of Medicinal Chemistry, 214, 113209.
22. World Health Organization. (2024). Cancer. https://www.who.int/news-room/fact-sheets/detail/cancer
23. Wu, L., Wang, X., Xu, W., Farzaneh, F., & Xu, R. (2009). The structure and pharmacological functions of coumarins. Current Medicinal Chemistry, 16(32), 4236–4260.
24. Xu, Z., Chen, L., Leung, L., Yen, G., Lee, C., & Chan, W. (2013). Structure-based drug design of kinase inhibitors. Current Topics in Medicinal Chemistry, 13(11), 1336–1347.
25. Yang, H., Lou, C., Sun, L., Li, J., Cai, Y., Wang, Z., ... & Tang, Y. (2019). admetSAR 2.0: Web-service for prediction and optimization of chemical ADMET properties. Nucleic Acids Research, 47(W1), W5–W14.
26. Yao, H., Price, T. T., Cantelli, G., Ngo, B., Warner, M. J., Olivere, L., ... & Kang, Y. (2020). Leukaemia hijacks a neural mechanism to invade the central nervous system. Nature, 585(7825), 55–60.
27. Zhang, J., Yang, P. L., & Gray, N. S. (2009). Targeting cancer with small molecule kinase inhibitors. Nature Reviews Cancer, 9(1), 28–39.
28. Zhang, Y., Li, X., Zou, D., Liu, W., Yang, J., Zhu, N., ... & Ning, G. (2008). Treatment of type 2 diabetes and dyslipidemia with the natural plant alkaloid berberine. Journal of Clinical Endocrinology & Metabolism, 93(7), 2559–2565.
29. Zhao, H., Caflisch, A., & Grütter, M. G. (2013). Molecular docking and virtual screening in drug discovery. Current Pharmaceutical Design, 19(30), 5390–5402.
30. Zhou, Y., Shen, J., Huang, Y., et al. (2022). Design, synthesis, and biological evaluation of novel coumarin derivatives with potent anticancer activity. Bioorganic Chemistry, 120, 105613.
31. Zubrienė, A., Matulis, D., & Tumkevičius, S. (2019). Coumarin derivatives as enzyme inhibitors and anticancer agents. Molecules, 24(4), 666.
32. Bray, F., Laversanne, M., Sung, H., Ferlay, J., Siegel, R. L., Soerjomataram, I., & Jemal, A. (2024). Global cancer statistics 2024: GLOBOCAN estimates of incidence and mortality worldwide. CA: A Cancer Journal for Clinicians, 74(3), 229–263.
33. Sung, H., Ferlay, J., Siegel, R. L., Laversanne, M., Soerjomataram, I., Jemal, A., & Bray, F. (2021). Global Cancer Statistics 2020: GLOBOCAN estimates of incidence and mortality worldwide for 36 cancers in 185 countries. CA: A Cancer Journal for Clinicians, 71(3), 209–249.